separations

MDPI

Article

The Effects of Outlet Diameter on Particle Movement and Separation Performance of the Cylindrical Hydrocyclone

Duanxu Hou [1], Haihao Wang [1], Daqing Hou [2], Hongying Zhu [1,*], Hongrun Song [1], Honghe Deng [1] and Qingguo Shao [1]

[1] School of Intelligent Manufacturing and Control Engineering, Shandong Institute of Petroleum and Chemical Technology, No. 500, Beier Road, Dongying District, Dongying 257061, China
[2] Luwa Coal Mine, Shandong Lutai Holding Group Co., Ltd., Jining 272300, China
* Correspondence: zhuhongying@sdipct.edu.cn

Abstract

The outlet diameter of hydrocyclones is a critical structural parameter that impacts product distribution and separation performance, drawing significant attention. In this paper, the separation efficiency and particle motion behavior in the cylindrical hydrocyclone with varying spigot diameters and vortex finder diameters are systematically analyzed using a TFM model. The numerical results indicate that a larger spigot diameter and a smaller vortex finder diameter reduce the axial velocity and expand the external swirling flow region, while a smaller spigot diameter and a larger vortex finder diameter enhance the particle circulation flow ratio and the coarse particle circulation flow proportion, thereby increasing the cut size. Slightly reducing the spigot diameter and increasing the vortex finder diameter enhances the separation accuracy. Nevertheless, for D_u = 0.075 D and $D_o \geq$ 0.4 D, the recovery rate in the underflow remains below 50% for all particle sizes, exhibiting severe particle misplacement and loss of separation efficiency. For D_u = 0.125 D, the reduction in coarse particle misplacement in the overflow is attributed to the abrupt changes in the coarse particle circulation flow proportion and medium particle circulation flow proportion. Generally, an appropriate coarse particle circulation flow proportion in the cylindrical hydrocyclone is beneficial for alleviating particle misplacement and improving separation accuracy.

Keywords: cylindrical hydrocyclone; outlet diameter; particle misplacement; separation accuracy

Academic Editor: Yundong Wang

Received: 10 April 2026
Revised: 11 May 2026
Accepted: 15 May 2026
Published: 17 May 2026

1. Introduction

Hydrocyclones are typical devices that accelerate particle separation utilizing centrifugal forces. Due to advantages such as small footprint, high separation efficiency, and high throughput, hydrocyclones are widely applied in particle separation operations in fields including mineral processing, chemical engineering, and environmental protection [1–3]. Despite the diverse geometric configurations of hydrocyclones, the fundamental principle underlying separation relies on the distinct movement patterns of discrete phases with different properties under the combined forces in the swirling flow field [4]. Under a specified feed pressure, particles are fed tangentially through the feed inlet into the separation chamber, forming a tangential flow under the guidance of the chamber walls [5,6]. Due to differences in particle properties, the magnitude of the radial resultant force acting on each solid particle is different. For finer particles, the centrifugal inertial force is insufficient to

counteract the drag force and centripetal buoyancy, causing the particles to move toward the center with the fluid and eventually be discharged through the overflow. For coarser particles, the centrifugal force is greater than the drag force and pressure gradient force, causing the particles to settle continuously toward the wall and eventually be discharged through the underflow. For medium particles, the centrifugal force is balanced by the sum of the drag force and the pressure gradient force, resulting in particles distributed in the internal swirling flow and the external swirling flow, ultimately being discharged through the overflow and the underflow.

The spigot diameter significantly impacts the separation performance of the hydrocyclone and directly determines the distribution and composition of the particles in the underflow [7]. The particle yield in the underflow and split ratio both increase gradually with increasing spigot diameter, while the cut size decreases [8]. An appropriate increase in the spigot diameter contributes to alleviating the misplaced coarse particle in the overflow and reduces the negative impact of increased feed size [9]. An undersized spigot diameter severely reduces the split ratio, resulting in excessive concentration in the underflow and even causing a "roping" phenomenon [10]. An oversized spigot diameter allows particles to bypass the separation process and be discharged directly through the underflow, exacerbating the fine particle misplaced phenomenon in the underflow and compromising separation performance [11]. Liu et al. compared the effects of elongated, double-cone, large-cone, step-cone, and anti-cone spigot configurations on the separation performance of hydrocyclones [12]. The findings indicate that the elongated spigot reduces the fine particle recovery rate in the underflow, thereby mitigating the misplacement of fine particles. Hou et al. observed that modestly increasing the upper diameter of the spigot improves separation precision and reduces particle misplacement [13]. In contrast, both oversized and undersized upper diameters exacerbate the misplacement of coarse particles in the overflow, thereby worsening separation performance. Jiang et al. designed a W-shaped spigot and evaluated its separation performance using numerical and physical experiments [14]. The W-shaped structure enables secondary separation at the bottom of the hydrocyclone, thereby reducing the fine particle recovery rate in the underflow, mitigating the fine particle misplacement, and improving separation efficiency. Han et al. observed that adding cylindrical and conical fixings to the spigot minimally impacts the fine particle separation efficiency but significantly reduces energy consumption [15].

The cut size gradually increases with increasing vortex finder diameter, and the particle recovery rate in the underflow gradually decreases [16]. Both undersized and oversized vortex finder diameters adversely affect the separation process [17]. The air core diameter exceeds the spigot diameter with an oversized vortex finder diameter, reducing the split ratio to zero and eliminating the separation effect [18,19]. Conversely, an undersized vortex finder diameter loses the air core, resulting in an excessively elevated split ratio, causing the hydrocyclone to forfeit its separation capability. Particles passing directly through the overflow without being separated can be reduced by inserting a vortex finder into the hydrocyclone, thereby minimizing the misplacement of coarse particles in the overflow [20]. Conversely, an excessively deeply inserted vortex finder reduces the separation space and shortens the particle residence time, thereby diminishing the separation efficiency for medium particles [21]. Research indicates that a thick-walled vortex finder can mitigate short-circuit flow and circulation flow in the surrounding region, thereby reducing the misplacement of coarse particles in the overflow [22,23]. Tang et al. evaluated the effects of vortex finder design on separation performance and concluded that the vortex finder diameter exerted the greatest effect, followed by the insertion depth, while the wall thickness exerted the least effect [24]. In recent years, numerous researchers have studied the design

of non-standard vortex finders and found that vortex finders with structures such as the mantle-shaped and the inverse conical can improve the separation performance [19,25,26]. Wang et al. replaced the vortex finder of the hydrocyclone with a tubular membrane for recovering valuable liquids and classifying particles [27]. Zhao et al. designed an annular vortex finder to address the short-circuit flow in cyclones and applied it to the separation of oil–water mixtures [28].

The advancement of testing technologies and optical instruments allows researchers to study the flow field and particle motion behavior in hydrocyclones, utilizing advanced equipment such as Particle Image Velocimetry (PIV) and Laser Doppler Anemometry (LDA) [29]. The advanced testing methods have further enhanced the understanding of the flow field characteristics and particle motion behavior in hydrocyclones [30]. However, these advanced testing methods primarily apply to lower concentration conditions, limiting the representativeness of the test results, while also incurring higher costs and requiring lengthy testing periods [31]. With the advancement of computational fluid dynamics and high-performance computing technologies, numerical simulation methods have gradually been widely applied to the study of cyclone separation processes, yielding numerous scientific achievements [32]. The separation process in hydrocyclones is a typical gas–liquid–solid multiphase flow, and simulating multiphase flow primarily involves two methods: the Eulerian–Eulerian and the Eulerian–Lagrangian methods [33]. In the Eulerian–Eulerian method, the two-fluid model considers each phase as a continuous phase interpenetrating the other and calculates the interactions between particles using the kinetic theory of granular flow [32,34]. As the most comprehensive model accounting for interphase interactions, the Eulerian–Eulerian method can theoretically be used to calculate the separation performance of hydrocyclones for all concentration levels [35]. The flow in the hydrocyclone is a strongly turbulent flow, and precisely selecting the turbulence model to accurately calculate such flow patterns is crucial for the accuracy of the calculation results [36]. The Reynolds Stress Model (RSM) and the Large Eddy Simulation (LES) method are the two models that can accurately describe the anisotropic turbulence in hydrocyclones [37]. The LES model directly simulates the large eddy structure, while the small-scale eddy is solved using a subgrid scale model, thus providing a more accurate prediction of the separation process compared to the RSM [38,39]. However, the LES model requires a finer mesh and smaller time steps, so it is still limited by computational speed in describing the separation process. The RSM is more widely used in simulating flow fields and particle motion in a hydrocyclone, considering both computational accuracy and efficiency.

The effect of outlet diameter on particle motion behavior and separation performance in cylindrical hydrocyclones is investigated using the TFM model. The particle velocity distribution, particle circulation flow, particle spatial distribution, and separation performance of cylindrical hydrocyclones with different outlet diameters are systematically analyzed. The study is expected to further enhance understanding of particle dynamics in cylindrical hydrocyclones and provide guidance for the structural design and optimization of cylindrical hydrocyclones.

2. Simulation Method and Conditions

2.1. Model Description

Despite the simple structure of the cylindrical hydrocyclone—where the separation chamber consists of a cylindrical section without a conical section—the internal flow field is extremely complicated owing to the turbulent flow. The simulation process is conducted in two stages to enhance the reliability of the numerical model. First, a two-phase flow field consisting of air and water is obtained using the TFM model. Based on this, particles are

released at the inlet, and the three-phase motion of particles, water, and air is simulated using the TFM model to characterize particle behavior and separation performance. The RSM is employed to describe anisotropic turbulence in hydrocyclones. Compared favorably to the LES model, the RSM offers higher computational efficiency and lower computational costs. A detailed description of the model can be found elsewhere [40].

2.2. Model Adaptability

It is essential to validate the accuracy and reliability of the model before conducting numerical experiments. Following the numerical simulation process, the validation of the numerical model is also conducted in two steps. First, the radial distributions of tangential velocity and axial velocity obtained from LDA experiments are contrasted with the numerical simulations to validate the gas–liquid flow model. Second, the gas–liquid–solid flow model is validated by comparing the partition curve obtained from laboratory experiments and numerical simulations. The validation results indicate that the model can accurately describe the flow field and separation performance of cylindrical hydrocyclones, at least for qualitative analysis. Detailed validation results can be found elsewhere [13]. Additionally, the model adopted in this study has been widely used to investigate the structural optimization of cylindrical hydrocyclones and explore the separation process [41].

2.3. Simulation Conditions

The particle motion behavior and separation performance of cylindrical hydrocyclones at different outlet diameters are examined to investigate the characteristics of the separation process. As depicted in Figure 1, a standard 200 mm cylindrical hydrocyclone is employed as the base structure, with the vortex finder diameter and spigot diameter serving as variables while all other structural parameters remain constant. The spigot diameters (D_u) adopted in this study are 0.075 D, 0.1 D, 0.125 D, 0.15 D, 0.175 D, 0.2 D, and 0.225 D; the vortex finder diameters (D_o) employed are 0.2 D, 0.25 D, 0.3 D, 0.35 D, 0.4 D, and 0.45 D. Among these, D_u = 0.15 D and D_o = 0.3 D are the spigot diameter and vortex finder diameter of the base hydrocyclone, respectively. The computational domain of the cylindrical hydrocyclone is divided into 178,882 hexahedral cells, with the mesh refined around the wall, the vortex finder, and the spigot to ensure that y+ is positioned within the log-law zone. The meshing scheme adopted for the 200 mm cyclone is grid-independent and convergent, and the detailed mesh configuration is illustrated in Figure 2.

In all cases, the inlet of the cylindrical hydrocyclone is configured as a velocity inlet. The inlet velocity of water and particles is set to 3 m/s based on the feed flow rate in the industrial application, and the volume fraction of the particle phase is set to 16.86% in accordance with the mass concentration of the feed in the industrial application. The two outlets of the cylindrical hydrocyclone are defined as pressure outlets, and the pressure at each outlet is assumed to be atmospheric pressure. Additionally, it is assumed that only the air phase can return to the computational domain through the two outlets. For water and air, non-slip boundary conditions are applied to the wall, while a specularity coefficient of 0.6 is adopted for the wall boundary conditions of the particle phase. The particle used is quartz particles with a density of 2630 kg/m^3. The originally measured quartz particle size distribution is categorized into seven representative size intervals, and the particle size distribution is simulated using seven discrete average particle sizes. Specific settings can be found elsewhere [40].

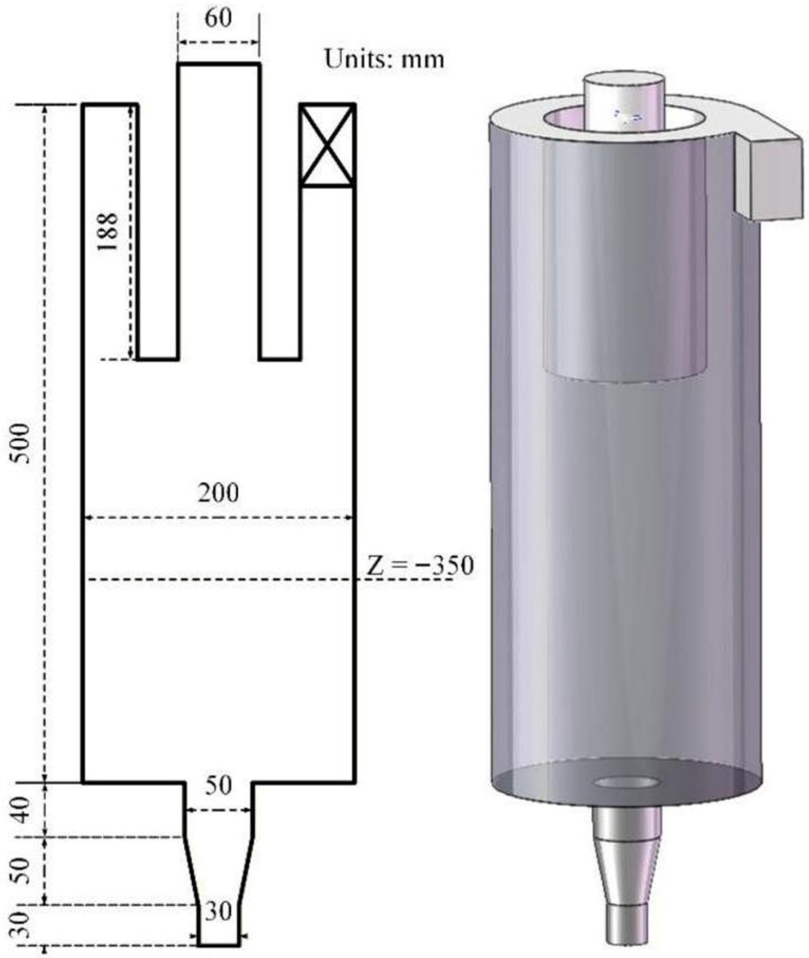

Figure 1. Geometrical parameters and diagram of the 200 mm cylindrical hydrocyclone.

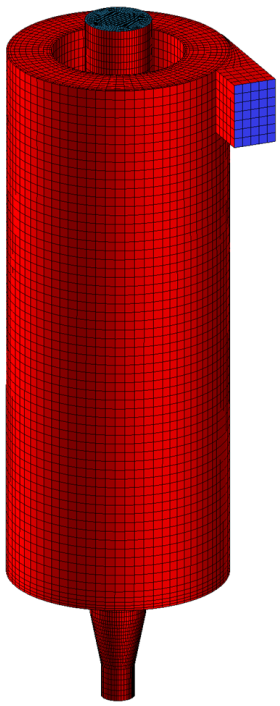

Figure 2. The computational mesh of the cylindrical hydrocyclone.

3. Results and Discussion

3.1. Partition Curve

The relationship between outlet diameter and the particle recovery rate in the underflow is presented in Figure 3. The fine particle recovery rate in the underflow increases gradually, while the coarse particle recovery rate in the underflow initially increases, then slightly decreases, and subsequently increases again with increasing spigot diameter. The recovery rate for each grain size in the underflow is below 50% at D = 0.075 D, exhibiting significant misplacement of coarse particles in the overflow, resulting in extremely poor separation efficiency of the hydrocyclone. The coarse particle recovery rate in the underflow suddenly increases at D_u = 0.125 D, and it is significantly higher than at D_u = 0.15 D and 0.17 D. As illustrated in Figure 3b, the recovery rate for each grain size in the underflow continuously decreases with increasing vortex finder diameter. When $D_o \geq 0.4$ D, the recovery rate for all grain sizes in the underflow is below 50%, rendering the cylindrical hydrocyclone essentially ineffective for separation, stemming from the low particle yield in the underflow. An inappropriate outlet diameter will cause severe particle misplacement, ultimately resulting in compromised separation performance of the cylindrical hydrocyclone. In summary, the outlet diameter significantly impacts the operational state of cylindrical hydrocyclones, with a relatively limited range for adjustment.

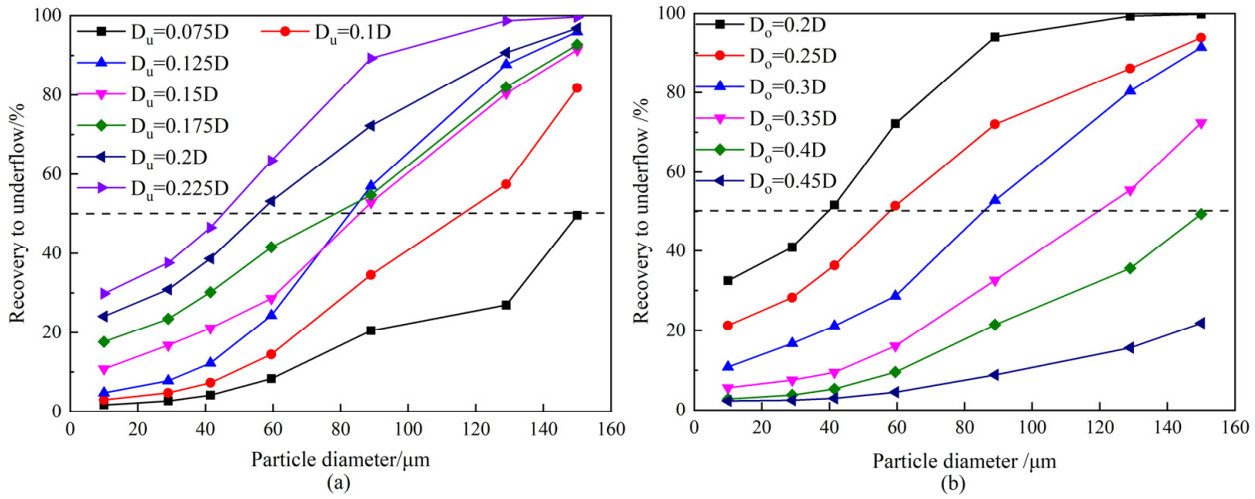

Figure 3. Effects of outlet diameter on partition curve: (**a**) spigot diameter; (**b**) vortex finder diameter.

To further analyze the effect of outlet diameter on separation efficiency, the cut size (d_{50}), the Ecart probable (Ep), and the imperfection value (I) are evaluated, and the results are presented in Tables 1 and 2. Notably, the hyphen (-) indicates that the Ep and I are uncalculable because the d_{75} and d_{25} values cannot be obtained from the partition curve, which signifies extremely suboptimal hydrocyclone separation performance and severe particle misplacement.

Table 1. Effects of spigot diameter on separation performance.

D_u	0.075 D	0.1 D	0.125 D	0.15 D	0.175 D	0.2 D	0.225 D
d_{50}/μm	>150	116.14	82.77	85.35	78.30	55.91	44.9
Ep/μm	-	34.69	26.37	35.12	43.64	41.63	-
I	-	0.3	0.32	0.41	0.56	0.74	-

Table 2. Effects of vortex finder diameter on separation performance.

D_o	0.2 D	0.25 D	0.3 D	0.35 D	0.4 D	0.45 D
d_{50}/μm	39.8	57.43	85.35	120.68	>150	>150
Ep/μm	-	38.86	35.12	-	-	-
I	-	0.68	0.41	-	-	-

According to Table 1, the d_{50} gradually decreases while the I gradually increases with increasing spigot diameter. Meanwhile, the Ep first decreases and then increases, reaching the minimum value at D_u = 0.125 D, indicating that a smaller spigot diameter may enhance the separation accuracy. Additionally, neither excessively oversized nor undersized spigot diameters allow calculation of the Ep and the I, indicating poor separation efficiency, with severe misplaced fine particles or misplaced coarse particles, respectively. It can be seen from Table 2 that the d_{50} gradually increases with increasing vortex finder diameter. The Ep and I can be calculated for D_o = 0.25 D and 0.3 D exclusively, indicating that the separation performance is extremely sensitive to the vortex finder diameter. Accordingly, inappropriate vortex finder diameters will exacerbate the misplacement of coarse particles and fine particles, potentially rendering the hydrocyclone ineffective. The Ep and the I both decrease as the vortex finder diameter increases from =0.25 D to =0.3 D, implying that suitably increasing the vortex finder diameter can improve separation accuracy.

3.2. Particle Velocity Distribution

3.2.1. Tangential Velocity

The effect of outlet diameter on the particle tangential velocity distribution at the Z = −350 mm is shown in Figure 4. It can be observed from Figure 4a that the spigot diameter has a relatively slight effect on the tangential velocity in the vicinity of the wall. However, the particle tangential velocity around the air core suddenly decreases as the spigot diameter increases from 0.125 D to 0.15 D. That is, an oversized spigot diameter reduces the tangential velocity around the air core, diminishing the centrifugal force on particles in this region. The observed abrupt change in the coarse particle recovery rate in the underflow at 0.125 D can be explained by this mechanism. Simultaneously, the tangential velocity peak gradually shifts toward the axis with increasing spigot diameter, reducing the tangential velocity gradient, which is disadvantageous for the misplaced coarse particles in the internal swirling flow region to return to the external swirling flow region. As shown in Figure 4b, the particle tangential velocity around the wall decreases slightly with increasing vortex finder diameter. In contrast, the particle tangential velocity around the air core first increases and then decreases with increasing vortex finder diameter. Additionally, the particle tangential velocity peak first increases and then decreases with increasing vortex finder diameter, resulting in the tangential velocity gradient first increasing and then decreasing. Greater tangential velocity gradients contribute to enhanced shear forces, thereby promoting coarse particles in the internal swirling flow region to return to the external swirling flow region, increasing separation accuracy. Additionally, it explains that appropriately increasing the vortex finder diameter can improve separation precision.

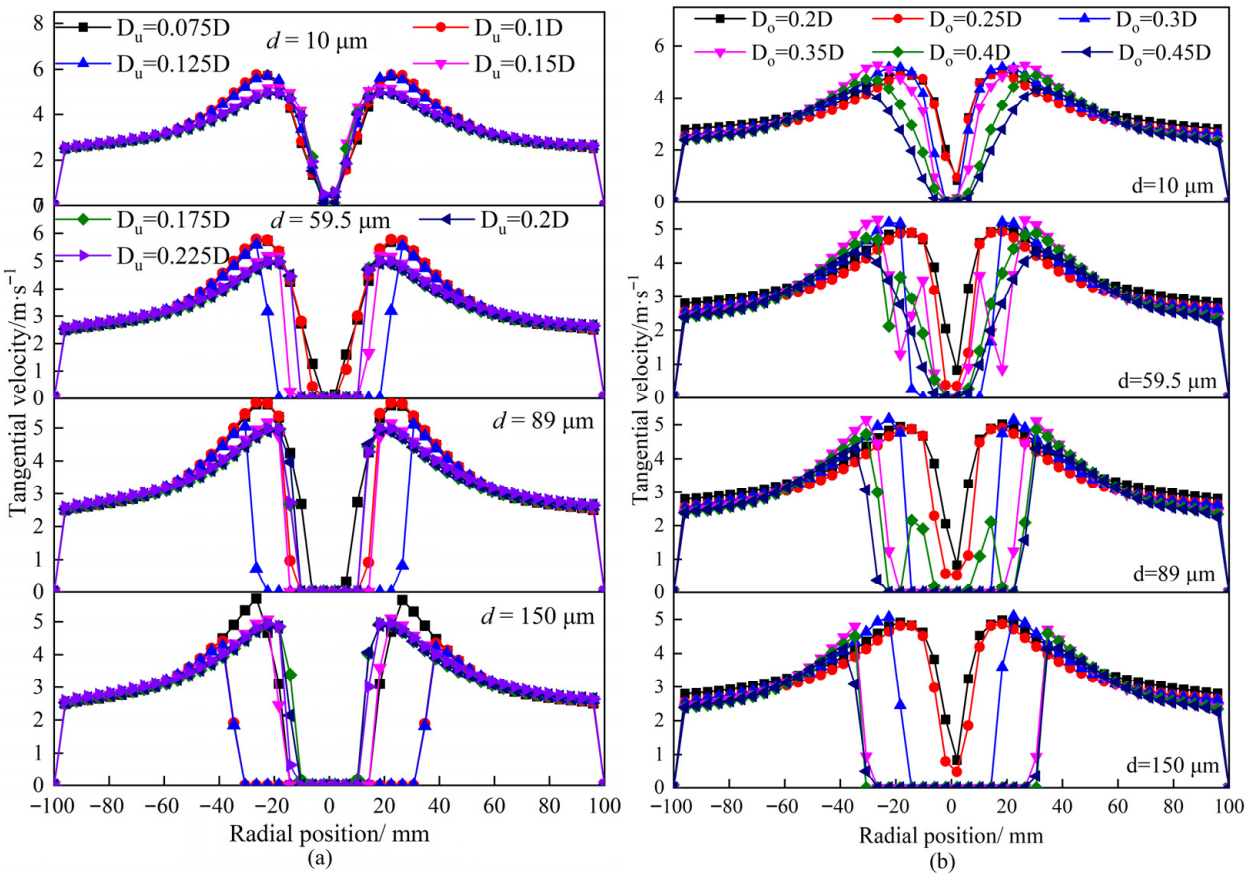

Figure 4. Effects of outlet diameter on the distribution of tangential velocity: (**a**) spigot diameter; (**b**) vortex finder diameter.

3.2.2. Axial Velocity

The effect of outlet diameter on the particle axial velocity distribution at the Z = −350 mm plane is presented in Figure 5. From Figure 5a, it can be observed that the particle axial velocity gradually decreases with increasing spigot diameter. The locus of zero vertical velocity tends to shift toward the axis, reducing the particle upward flow region. As a result, the upward particle flow rate decreases with increasing spigot diameter, whereas the particle yield in the underflow gradually increases. Simultaneously, the point of maximum axial velocity shifts toward the axis with increasing spigot diameter, potentially indicating a reduction in particle residence time in the region proximate to the air core. Furthermore, the impact of spigot diameter on particle axial velocity around the air core diminishes with increasing particle size, attributable to the distribution of particle volume fraction in this region. According to Figure 5b, the particle axial velocity gradually increases with the increase in the vortex finder diameter. The locus of zero vertical velocity shifts toward the wall, increasing the internal swirling flow region with upward axial velocity and expanding the particle upward flow region. The particle axial velocity remains essentially unchanged with increasing vortex finder diameter at $D_o \geq 0.4$ D. The impact of the vortex finder diameter on the particle axial velocity increases with increasing particle size. Conversely, the vortex finder diameter significantly impacts the particle axial velocity compared to the spigot diameter, thereby affecting the particle yield in the underflow.

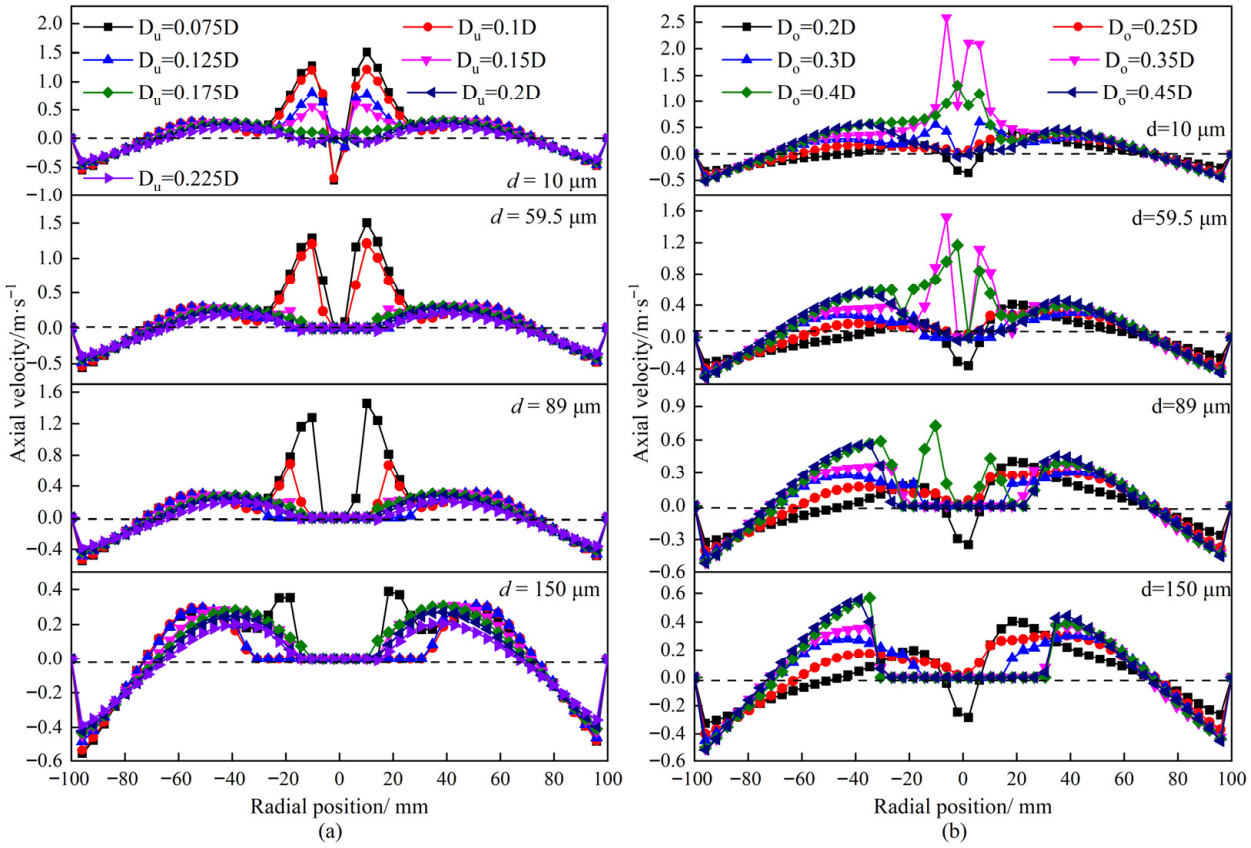

Figure 5. Effects of outlet diameter on the distribution of axial velocity: (**a**) spigot diameter; (**b**) vortex finder diameter.

3.3. Particle Circulation Flow

3.3.1. Downward Flow Ratio and Upward Flow Ratio

The particle circulation flow is characterized by the downflow flow ratio and the upward flow ratio. The downward flow ratio and the upward flow ratio are defined as the ratio of the particle moving with the external swirling flow and the particle moving with the internal swirling flow to the inlet flow at a specific axial section, respectively. The detailed methods for calculating the downward flow ratio and the upward flow ratio can be found in the Supplementary File.

The effect of outlet diameter on the particle downward flow ratio is illustrated in Figure 6. As evident from Figure 6a, the 10 μm particle downward flow ratio decreases with decreasing axial position for different spigot diameters, indicating no significant fine particle circulation flow is formed. For $D_u \geq 0.175$ D, both the 59.5 μm and 89 μm particle downward flow ratios initially increase and then decrease with decreasing axial position at the bottom of the separation chamber and below the vortex finder. Furthermore, a substantially slow-changing region for 59.5 μm and 89 μm particle downward flow ratios exists in the middle section of the hydrocyclone, forming a distinct medium particle circulation flow. The 150 μm particle downward flow ratio increases initially and then decreases with decreasing axial position for different spigot diameters, indicating the formation of a pronounced coarse particle circulation flow. As shown in Figure 6b, the 10 μm particle downward flow ratio in the bottom region of the separation chamber first increases and then decreases at D_o = 0.2 D, thereby forming a prominent fine particle circulation flow. The 59.5 μm and 89 μm particle downward flow ratio generally increases with increasing vortex finder diameter. Notably, a pronounced particle circulation flow forms in the bottom region of the separation chamber for $D_o \leq 0.25$ D. However, both

59.5 μm and 89 μm particle downward flow ratio changes slowly in the middle region of the separation chamber, indicating the formation of a medium particle circulation flow. The 150 μm particle downward flow ratio exhibits an initial increase followed by a decrease with decreasing axial position across different vortex finder diameters, resulting in significant coarse particle recirculation.

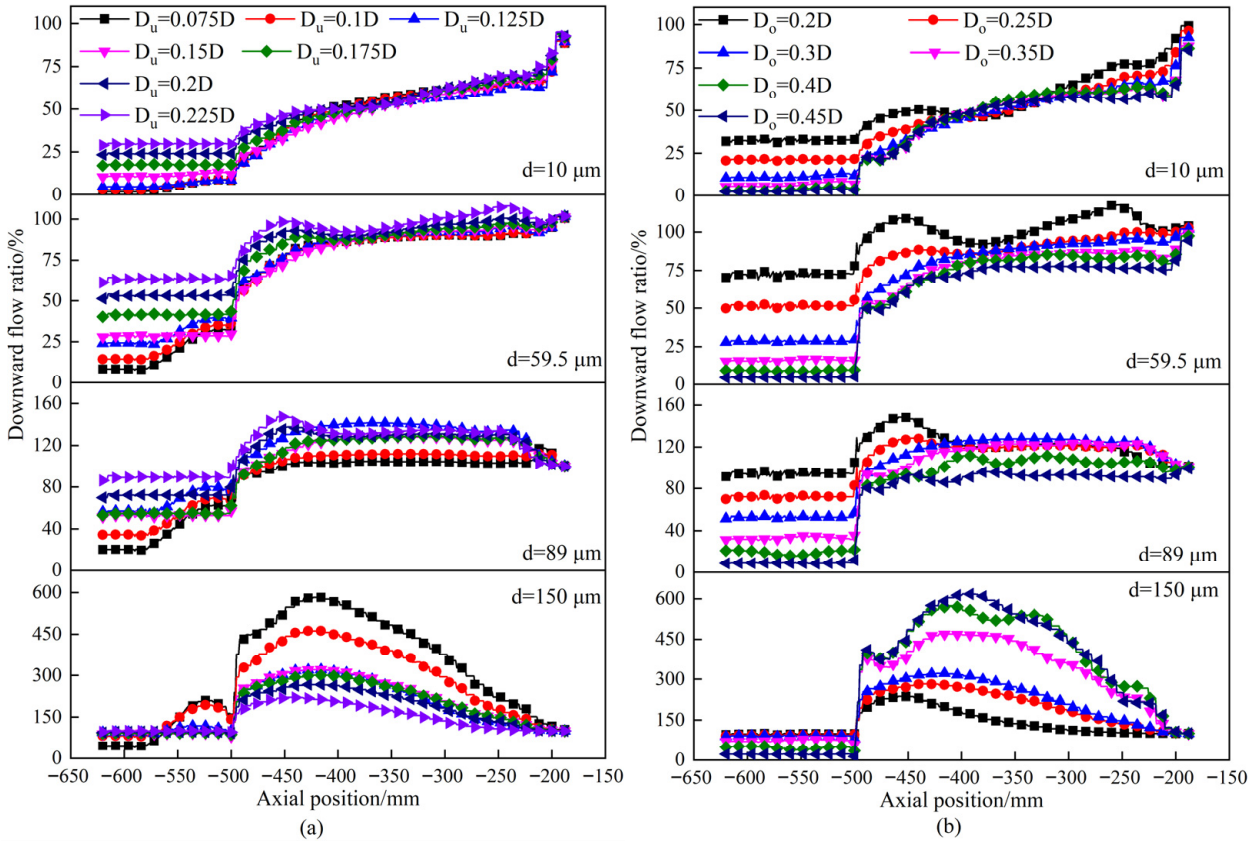

Figure 6. Effects of outlet diameter on the downward flow ratio: (**a**) spigot diameter; (**b**) vortex finder diameter.

The effect of outlet diameter on the upward flow ratio is depicted in Figure 7. According to Figure 7a, the particle upward flow ratio gradually decreases with increasing spigot diameter, diminishing the potential for particles to move with the internal swirling flow. Moreover, the coarse particle upward flow ratio peak progressively shifts toward the spigot, which contributes to alleviating the misplaced particle in the overflow. For $D_u \leq 0.125$ D, particle circulation forms in the spigot due to limited throughput capacity resulting from an excessively small spigot diameter. Simultaneously, the particle circulation in the spigot reduces the fine particle recovery rate in the underflow, thereby minimizing the misplacement of fine particles in the underflow. From Figure 7b, it can be seen that the particle upward flow ratio gradually increases with increasing vortex finder diameter, accompanied by an increase in the amount of particles moving with the internal swirling flow. Simultaneously, at $D_o \geq 0.125$ D, the maximum upward flow ratio for 150 μm particles exceeds 300% while a majority of coarse particles are entrained by the internal swirling flow. Consequently, severe mixing of coarse and fine particles forms in the internal swirling flow region, causing the hydrocyclone to fail in separating particles, thereby preventing the attainment of the d_{75} value in the partition curve. Furthermore, the maximum particle upward flow ratio gradually shifts toward the vortex finder, which is not conducive to alleviating the misplacement of coarse particles in the overflow.

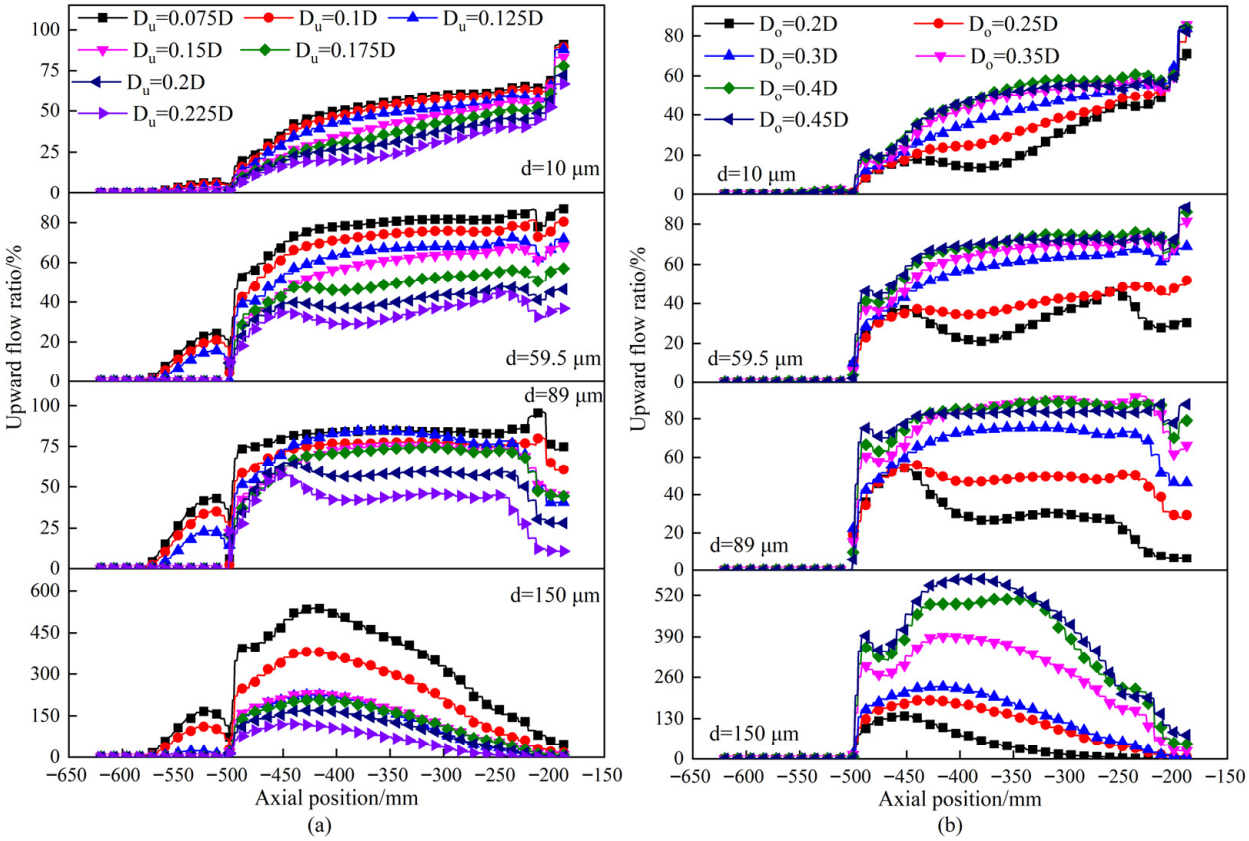

Figure 7. Effects of outlet diameter on the upward flow ratio: (**a**) spigot diameter; (**b**) vortex finder diameter.

3.3.2. Circulation Flow Ratio and Circulation Flow Proportion

To better evaluate the impact of outlet diameter on particle circulation flow in cylindrical hydrocyclones, the particle circulation flow ratio and the proportion of particle circulation flow are examined. The particle circulation flow ratio can be applied to evaluate the total particle circulation flow in a hydrocyclone, representing the ratio of the total particle circulation flow rate in the hydrocyclone to the total particle flow rate in the feed. The particle circulation flow proportion is employed to evaluate the particle size distribution of the circulation flow, representing the ratio of the particle mass flow rate that traverses the locus of zero vertical velocity from the internal swirling flow region to the external swirling flow region to the total particle circulation flow rate. The detailed methods for calculating the particle circulation flow ratio and particle circulation flow proportion are provided in the Supplementary File.

The effect of outlet diameter on the particle circulation flow ratio in the cylindrical hydrocyclone is depicted in Figure 8. As observed in Figure 8a, the particle circulation flow ratio gradually decreases with increasing spigot diameter. An increase in the spigot diameter broadens the flow passage of the spigot, enhancing the particle yield in the underflow, which reduces the upward flow ratio. Meanwhile, the relatively minor variation in tangential velocity results in negligible changes in centrifugal force, gradually diminishing the amount of particles returning from the internal swirling flow region to the external swirling flow region to contribute to the circulation. As depicted in Figure 8b, the particle circulation flow ratio increases initially and then decreases with increasing vortex finder diameter, reaching the maximum at D_o = 0.35 D. The particle upward flow ratio increases with increasing vortex finder diameter, consequently increasing the number of particles participating in circulation. For D_o > 0.35 D, persistent decreases in centrifugal force and in-

creases in axial velocity within the internal swirling flow reduce the probability of particles forming circulation flows.

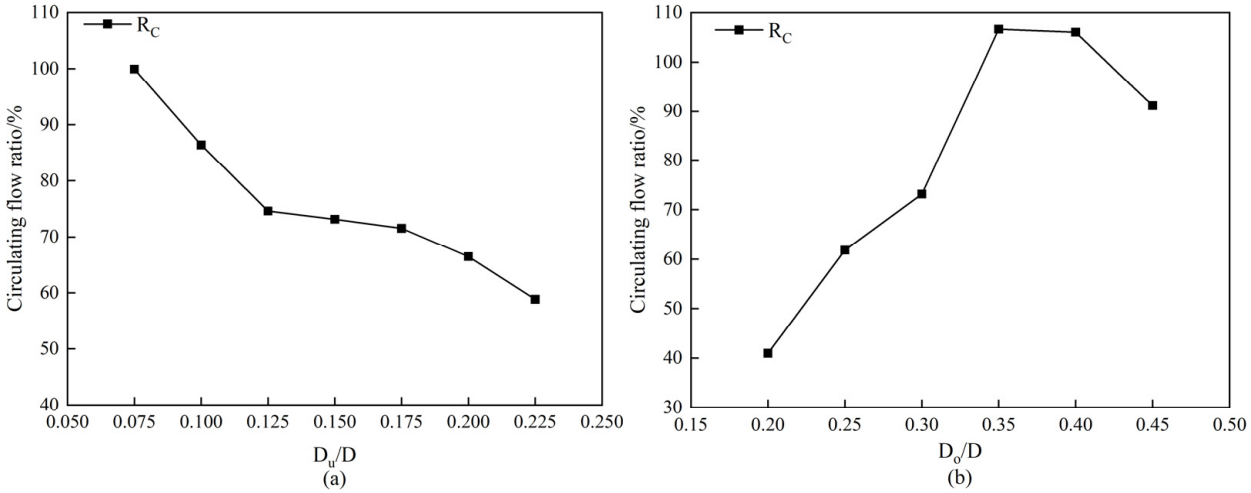

Figure 8. Effects of outlet diameter on the circulation flow ratio: (**a**) spigot diameter; (**b**) vortex finder diameter.

Figure 9 demonstrates the relationship between outlet diameter and the particle circulation proportion in the cylindrical hydrocyclone. As seen in Figure 9a, the fine particle circulation flow proportion increases continuously with the increase in the spigot diameter, while the medium particle circulation flow proportion increases initially, then decreases, and finally increases again. Conversely, the coarse particle circulation flow proportion decreases initially, then increases, and finally decreases again, indicating that appropriately increasing the spigot diameter can strengthen medium particle circulation flow while reducing coarse particle circulation flow. For D_u = 0.125 D, the coarse particle circulation flow proportion is slightly larger than that for D_u = 0.225 D, while the medium particle circulation flow proportion is slightly smaller, which may explain the sharp increase in the coarse particle recovery rate in the underflow observed in Figure 3a for D_u = 0.125 D. According to Figure 9b, the fine and medium particle circulation flow proportion decreases continuously as the vortex finder diameter increases, while the coarse particle circulation flow proportion increases continuously, implying that an increase in vortex finder diameter enhances the coarse particle circulation flow. For $D_o \geq 0.4$ D, the coarse particle circulation flow proportion exceeds 80%, leading to substantial accumulation of coarse particles in the hydrocyclone and significant misplacement of coarse particles in the overflow, ultimately resulting in the coarse particle recovery rate in the underflow being below 50% in Figure 3b. The coarse particle circulation flow dominates under all outlet diameter conditions except for excessively oversized spigot diameters and undersized vortex finder diameters. Based on the comparison with the partition curve, a certain coarse particle circulation flow is crucial for maintaining a larger cut size and higher separation precision.

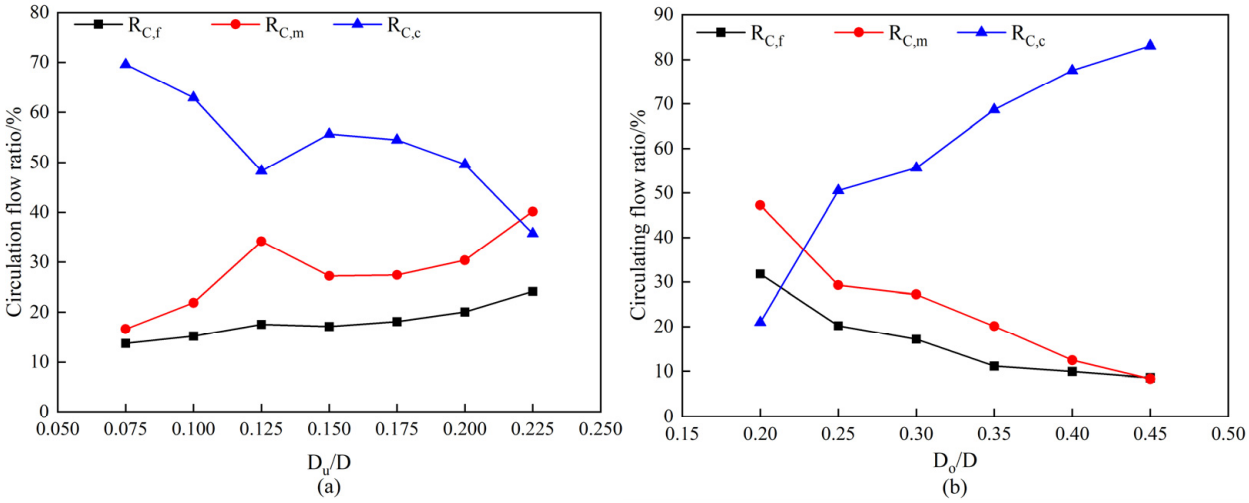

Figure 9. Effects of outlet diameter on the circulation flow proportion: (**a**) spigot diameter; (**b**) vortex finder diameter.

3.4. Particle Size Distribution

The particle spatial distribution in the hydrocyclone is intimately related to the separation behavior, and the particle distribution characteristics at different outlet diameters are further examined. The enrichment ratio is employed to evaluate the particle distribution in the cyclone, defined as the particle volume fraction in the local grid divided by the reference particle volume fraction in the feed.

The effect of outlet diameter on particle enrichment ratio is presented in Figure 10. The 10 μm particles primarily accumulate in the region surrounding the air core under all outlet diameter conditions, while the 59.5 μm and 89 μm particles accumulate around the wall and the air core. In contrast, the 150 μm particles accumulate in multiple regions of the separation chamber, and the outlet diameter exhibits negligible impact on the particle accumulation regions. As observed in Figure 10a, the peak of the medium particles and coarse particles enrichment ratio in the separation chamber shifts toward the wall first and then toward the center as the spigot diameter increases. Notably, the peak of particle enrichment ratio is nearest to the wall at D_u = 0.125 D, which further elucidates the reason for the abrupt changes in cut size and separation precision. Simultaneously, the coarser particle enrichment ratio increases as the spigot diameter decreases, contributing to the misplacement phenomenon of coarse particles in the overflow. As observed in Figure 10b, the enrichment ratio of particles with d $\leq$ 89 μm increases with an increase in the vortex finder diameter in the region surrounding the air core, while decreasing in other regions, and increasing the cut size. Additionally, the coarser particle enrichment ratio increases with increasing vortex finder diameter. Although the peak of the coarse particle enrichment ratio shifts toward the wall with increasing vortex finder diameter, the coarse particle enrichment ratio in the region beneath the vortex finder gradually increases, contributing to an enlargement of the cut size.

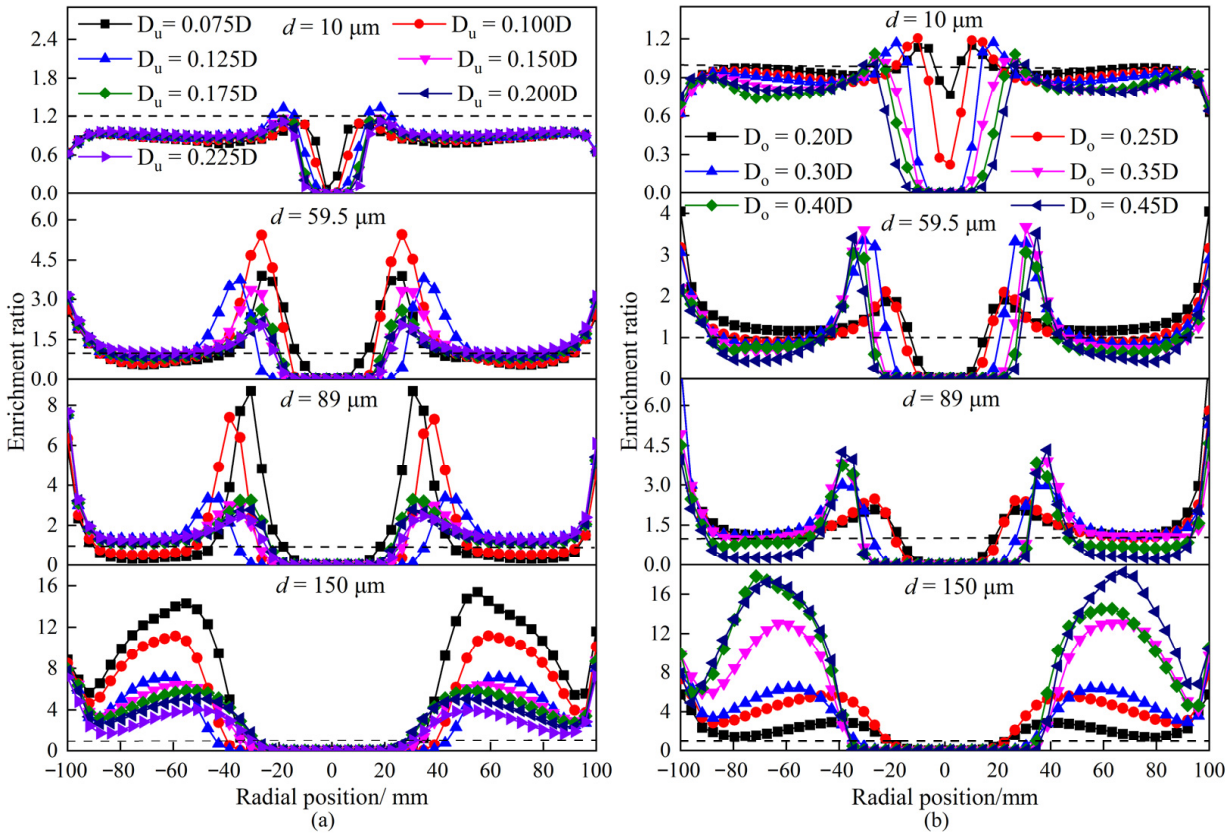

Figure 10. Effects of outlet diameter on the enrichment ratio: (**a**) spigot diameter; (**b**) vortex finder diameter.

4. Conclusions

The effects of the outlet diameter of a cylindrical hydrocyclone on particle kinetic behavior are investigated by varying the spigot diameter and the vortex finder diameter, respectively. The main findings of this study are summarized as follows:

1. Except for D_u = 0.125 D, either increasing the spigot diameter or decreasing the vortex finder diameter increases the particle recovery rate in the underflow. With D_u = 0.075 D and $D_o \geq$ 0.4 D, the particle recovery rate for every size in the underflow is below 50%, resulting in severe particle misplacement.
2. Both reducing the spigot diameter and increasing the vortex finder diameter increase the cut size, but appropriately reducing the spigot diameter and appropriately increasing the vortex finder diameter contribute to minimizing Ep and I, enhancing the separation accuracy.
3. The impact of outlet diameter on particle tangential velocity is concentrated in the region around the air core. Increasing the spigot diameter and decreasing the vortex finder diameter both reduce the particle axial velocity, promoting the LZVV migration toward the axis, thereby increasing the particle recovery rate in the underflow.
4. Decreasing the spigot diameter and increasing the vortex finder diameter increase the circulation flow ratio and the coarse particle circulation flow proportion, thereby increasing the coarse particle enrichment ratio and consequently increasing the separation size.

Supplementary Materials: The following supporting information can be downloaded at: https://www.mdpi.com/article/10.3390/separations13050151/s1, Figure S1: Grid-independence check; Figure S2: Comparison of distributions of the tangential velocities (a) and axial velocities (b); Figure S3: Comparison of the simulated and measured partition curves.

Author Contributions: Methodology, Q.S.; Software, H.Z., H.S. and Q.S.; Validation, D.H. (Daqing Hou), H.Z. and H.D.; Formal analysis, D.H. (Duanxu Hou), H.W., H.Z. and H.D.; Investigation, D.H. (Duanxu Hou) and H.D.; Resources, D.H. (Daqing Hou); Data curation, H.S.; Writing—original draft, D.H. (Duanxu Hou), H.W. and H.S.; Visualization, H.D.; Supervision, Q.S.; Funding acquisition, D.H. (Duanxu Hou), H.Z. and Q.S. All authors have read and agreed to the published version of the manuscript.

Funding: This work was funded by the National Natural Science Foundation of China (No. 22508232), the Dongying Science Development Fund (No. DJB20240036), and the Taishan Scholars Program of Shandong Province (No. tsqn202507273).

Data Availability Statement: The original contributions presented in this study are included in the article/Supplementary Material. Further inquiries can be directed to the corresponding author.

Conflicts of Interest: Author Daqing Hou was employed by the Luwa Coal Mine, Shandong Lutai Holding Group Co., Ltd. The remaining authors declare that the research was conducted in the absence of any commercial or financial relationships that could be construed as a potential conflict of interest.

References

1. Wei, Q.; Xiong, Z.; Zhao, J.; Huang, Y.; Huang, Y.; Lv, W.; Wang, H. In-situ reduction of heavy metal contaminated soil by hydrocyclone based on axial sorting of particles. *J. Hazard. Mater.* **2025**, *491*, 137912. [CrossRef] [PubMed]
2. Tsamoutsoglou, K.; Kechagias, A.; Katzourakis, V.E.; Chrysikopoulos, C.V.; Gikas, P. Investigation and efficiency estimation of a hydrocyclone for the treatment of primary municipal wastewater. *J. Environ. Manag.* **2025**, *380*, 125134. [CrossRef]
3. Trisap, W.; Photaworn, S.; Khongprom, P. Impact of Hydrocyclone Geometry on Glycerol Separation Efficiency in Biodiesel Purification. *Int. J. Chem. Eng.* **2025**, *2025*, 1758062. [CrossRef]
4. Pukkella, A.K.; Vega-Garcia, D.; Hadler, K.; Cilliers, J. The influence of surface-wall roughness on hydrocyclone performance. *Sep. Purif. Technol.* **2025**, *360*, 131109. [CrossRef]
5. Hwang, K.-J.; Wu, W.-H.; Qian, S.; Nagase, Y. Nagase†, CFD Study on the Effect of Hydrocyclone Structure on the Separation Efficiency of Fine Particles. *Sep. Sci. Technol.* **2008**, *43*, 3777–3797. [CrossRef]
6. Liu, X.-L.; Chen, J.-Y.; Cao, M.-Q.; Ma, X.; Zhang, H.-B. Study on the effect of particle shape on underflow entrainment in hydrocyclone. *Sep. Sci. Technol.* **2025**, *60*, 723–736. [CrossRef]
7. Gonçalves, M.S.; Barrozo, M.A.S.; Vieira, L.G.M. Effects of Solids Concentration and Underflow Diameter on the Performance of a Newly Designed Hydrocyclone. *Chem. Eng. Technol.* **2017**, *40*, 1750–1757. [CrossRef]
8. Xu, Y.; Song, X.; Sun, Z.; Tang, B.; Li, P.; Yu, J. Numerical Investigation of the Effect of the Ratio of the Vortex-Finder Diameter to the Spigot Diameter on the Steady State of the Air Core in a Hydrocyclone. *Ind. Eng. Chem. Res.* **2013**, *52*, 5470–5478. [CrossRef]
9. Kyriakidis, Y.N.; Silva, D.O.; Barrozo, M.A.S.; Vieira, L.G.M. Effect of variables related to the separation performance of a hydrocyclone with unprecedented geometric relationships. *Powder Technol.* **2018**, *338*, 645–653. [CrossRef]
10. Zhang, C.; Cui, B.; Wei, D.; Lu, S. Effects of underflow orifice diameter on the hydrocyclone separation performance with different feed size distributions. *Powder Technol.* **2019**, *355*, 481–494. [CrossRef]
11. Tian, J.; Ni, L.; Song, T.; Shen, C.; Yao, Y.; Zhao, J. Numerical study of foulant-water separation using hydrocyclones enhanced by reflux device: Effect of underflow pipe diameter. *Sep. Purif. Technol.* **2019**, *215*, 10–24. [CrossRef]
12. Liu, P.; Chen, B.; Hou, D.; Yang, X.; Zhang, W.; Lu, Y. Designing the Spigot Structure of Hydrocyclones to Reduce Fine Particle Misplacement in Underflow. *Water* **2024**, *16*, 1070. [CrossRef]
13. Hou, D.; Cui, B.; Zhao, Q.; Wei, D.; Song, Z.; Feng, Y. Research on the structure of the cylindrical hydrocyclone spigot to mitigate the misplacement of particles. *Powder Technol.* **2021**, *387*, 61–71. [CrossRef]
14. Jiang, L.; Liu, P.; Yang, X.; Zhang, Y.; Li, X.; Zhang, Y.; Wang, H. Effect of Overflow Pipe on the Internal Flow Fields and Separation Performance of W-Shaped Hydrocyclones. *Minerals* **2020**, *10*, 329. [CrossRef]
15. Han, T.; Liu, H.; Xiao, H.; Chen, A.; Huang, Q. Experimental study of the effects of apex section internals and conical section length on the performance of solid–liquid hydrocyclone. *Chem. Eng. Res. Des.* **2019**, *145*, 12–18. [CrossRef]
16. Vega-Garcia, D.; Cilliers, J.J.; Brito-Parada, P.R. CFD modelling of particle classification in mini-hydrocyclones. *Sep. Purif. Technol.* **2020**, *251*, 117253. [CrossRef]
17. Vieira, L.G.; Barrozo, M.A. Effect of vortex finder diameter on the performance of a novel hydrocyclone separator. *Miner. Eng.* **2014**, *57*, 50–56. [CrossRef]
18. Su, T.; Zhang, Y. Effect of the Vortex Finder and Feed Parameters on the Short-Circuit Flow and Separation Performance of a Hydrocyclone. *Processes* **2022**, *10*, 771. [CrossRef]

19. Ghodrat, M.; Kuang, S.; Yu, A.; Vince, A.; Barnett, G.; Barnett, P. Numerical analysis of hydrocyclones with different vortex finder configurations. *Miner. Eng.* **2014**, *63*, 125–138. [CrossRef]
20. Martínez, L.F.; Lavín, A.G.; Mahamud, M.M.; Bueno, J.L. Vortex finder optimum length in hydrocyclone separation. *Chem. Eng. Process. Process Intensif.* **2008**, *47*, 192–199. [CrossRef]
21. Tian, J.; Ni, L.; Song, T.; Zhao, J. CFD simulation of hydrocyclone-separation performance influenced by reflux device and different vortex-finder lengths. *Sep. Purif. Technol.* **2020**, *233*, 116013. [CrossRef]
22. Zhao, Q.; Cui, B.; Wei, D.; Song, T.; Feng, Y. Numerical analysis of the flow field and separation performance in hydrocyclones with different vortex finder wall thickness. *Powder Technol.* **2019**, *345*, 478–491. [CrossRef]
23. Wu, Z.; Liang, Z.; Li, P.; Li, F.; Yang, H. Effect of Vortex Finder Wall Thickness on Internal Flow Field and Classification Performance in a Hydrocyclone. *Separations* **2025**, *12*, 149. [CrossRef]
24. Tang, B.; Xu, Y.; Song, X.; Sun, Z.; Yu, J. Numerical study on the relationship between high sharpness and configurations of the vortex finder of a hydrocyclone by central composite design. *Chem. Eng. J.* **2015**, *278*, 504–516. [CrossRef]
25. Wang, B.; Yu, A. Numerical study of the gas–liquid–solid flow in hydrocyclones with different configuration of vortex finder. *Chem. Eng. J.* **2008**, *135*, 33–42. [CrossRef]
26. Hwang, K.-J.; Chou, S.-P. Designing vortex finder structure for improving the particle separation efficiency of a hydrocyclone. *Sep. Purif. Technol.* **2017**, *172*, 76–84. [CrossRef]
27. Wang, C.-C.; Wu, R.-M. Experimental and simulation of a novel hydrocyclone-tubular membrane as overflow pipe. *Sep. Purif. Technol.* **2018**, *198*, 60–67. [CrossRef]
28. Zhao, W.; Li, J.-P.; Zhang, T.; Wei, A.-S.; Li, S.-Y.; Yang, D.-H.; Yang, X.-J.; Jiang, X.; Wang, H. Separation characters of dewatering hydrocyclone with annular vortex finder based on particle image velocimetry and experiments. *Sep. Purif. Technol.* **2025**, *353*, 128619. [CrossRef]
29. Quteishat, M.A.K. Hydrocyclone flow characteristics and measurements. *Flow Meas. Instrum.* **2020**, *73*, 101741. [CrossRef]
30. Marins, L.P.; Duarte, D.G.; Loureiro, J.B.; Moraes, C.A.; Freire, A.S. LDA and PIV characterization of the flow in a hydrocyclone without an air-core. *J. Pet. Sci. Eng.* **2010**, *70*, 168–176. [CrossRef]
31. Chang, Y.F.; Ilea, C.G.; Aasen, Ø.L.; Hoffmann, A.C. Particle flow in a hydrocyclone investigated by positron emission particle tracking. *Chem. Eng. Sci.* **2011**, *66*, 4203–4211. [CrossRef]
32. Dianyu, E.; Fan, H.; Su, Z.; Xu, G.; Zou, R.; Yu, A.; Kuang, S. Numerical study of the multiphase flows and separation performance of hydrocyclone with tapered cross-section inlet. *Powder Technol.* **2023**, *416*, 118208.
33. Fang, X.; Wang, G.; Zhong, L.; Qiu, S.; Wang, D. A CFD–DEM analysis of the de-cementation behavior of weakly cemented gas hydrate–bearing sediments in a hydrocyclone separator. *Part. Sci. Technol.* **2022**, *40*, 812–823. [CrossRef]
34. Ghodrat, M.; Qi, Z.; Kuang, S.B.; Ji, L.; Yu, A.B. Computational investigation of the effect of particle density on the multiphase flows and performance of hydrocyclone. *Miner. Eng.* **2016**, *90*, 55–69. [CrossRef]
35. Dianyu, E.; Xu, G.; Fan, H.; Cui, J.; Tan, C.; Zhang, Y.; Zou, R.; Kuang, S.; Yu, A. Numerical investigation of hydrocyclone inlet configurations for improving separation performance. *Powder Technol.* **2024**, *434*, 119384. [CrossRef]
36. Vakamalla, T.R.; Mangadoddy, N. Numerical simulation of industrial hydrocyclones performance: Role of turbulence modelling. *Sep. Purif. Technol.* **2017**, *176*, 23–39. [CrossRef]
37. Corrêa, R.G.; Andrade, J.R.; de Souza, F.J. Improving Separation Prediction of Cyclone Separators with a Hybrid URANS-LES Turbulence Model. *Powders* **2023**, *2*, 607–623. [CrossRef]
38. Zhang, S.; Zhao, L.; Zhou, L.; Liu, L.; Jiang, M. Numerical and experimental study on enhanced oil–water separation performance using hydrocyclone coupled with particles. *Phys. Fluids* **2023**, *35*, 113331. [CrossRef]
39. Martins, D.A.d.M.; Andrade, J.R.; Duarte, C.A.R.; Salvo, R.d.V.; de Souza, F.J. A Large Eddy Simulation Study of Cyclones: The Effects of Interparticle Collisions on Erosion Prediction. *J. Energy Power Technol.* **2022**, *4*, 17. [CrossRef]
40. Hou, D.; Zhao, Q.; Liu, P.; Jiang, L.; Cui, B.; Wei, D. Effects of bottom profile on the circulation and classification of particles in cylindrical hydrocyclones. *Adv. Powder Technol.* **2023**, *34*, 104050. [CrossRef]
41. Hou, D.; Zhao, Q.; Cui, B.; Wei, D.; Song, Z.; Feng, Y. Geometrical configuration of hydrocyclone for improving the separation performance. *Adv. Powder Technol.* **2022**, *33*, 103419. [CrossRef]